Article

Cell Reports

# Impairment of Release Site Clearance within the Active Zone by Reduced SCAMP5 Expression Causes Short-Term Depression of Synaptic Release

## Graphical Abstract

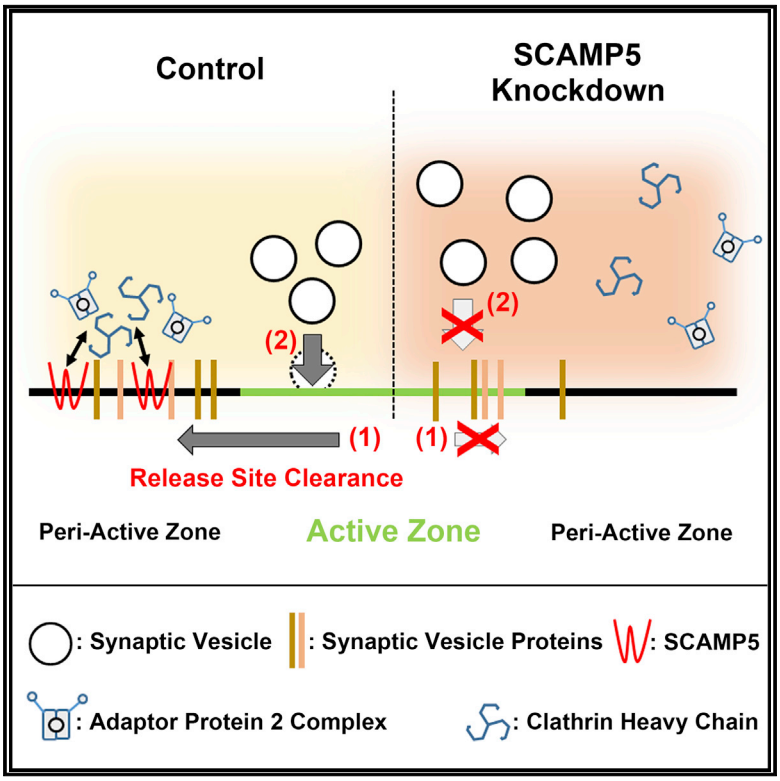


## Highlights

- SCAMP5 directly interacts with AP2 via a noncanonical site located in its 2/3 loop
- SCAMP5 KD induces faster synaptic depression and slower recovery after depression
- SCAMP5 KD causes strong frequency-dependent short-term synaptic depression
- Such synaptic defects in SCAMP5 KD are due to inefficient release site clearance

## Authors

Daehun Park, Unghwi Lee, Eunji Cho, ..., Won-Kyung Ho, Kwangwook Cho, Sunghoe Chang

## Correspondence

sunghoe@snu.ac.kr

## In Brief

Park et al. show that SCAMP5 plays an important role in release site clearance during intense neuronal activity. Loss of SCAMP5 results in a traffic jam at release sites, causing aberrant short-term synaptic depression that might be associated with the synaptic dysfunction observed in autism.

Park et al., 2018, Cell Reports 22, 3339–3350
March 20, 2018 
https://doi.org/10.1016/j.celrep.2018.02.088

CellPress

Cell Reports
Article



# Impairment of Release Site Clearance within the Active Zone by Reduced SCAMP5 Expression Causes Short-Term Depression of Synaptic Release

Daehun Park,[1] Unghwi Lee,[1] Eunji Cho,[1] Haiyan Zhao,[2] Jung Ah Kim,[1,3] Byoung Ju Lee,[1] Philip Regan,[4] Won-Kyung Ho,[1,5] Kwangwook Cho,[4,6] and Sunghoe Chang[1,3,5,7,*]

[1]Department of Physiology and Biomedical Sciences, Seoul National University College of Medicine, Seoul, South Korea
[2]Physical Examination Center, Department of Internal Medicine, Yanbian University Hospital, Yanji, Jilin Province, China
[3]Neuroscience Research Institute, Medical Research Center, Seoul National University College of Medicine, Seoul, South Korea
[4]Bristol Medical School, Faculty of Health Sciences, University of Bristol, Bristol, UK
[5]Biomembrane Plasticity Research Center, Seoul National University College of Medicine, Seoul, South Korea
[6]Present address: Department of Basic and Clinical Neuroscience, Institute of Psychiatry, Psychology and Neuroscience, King's College London, London, UK
[7]Lead Contact
*Correspondence: sunghoe@snu.ac.kr
https://doi.org/10.1016/j.celrep.2018.02.088

## SUMMARY

**Despite being a highly enriched synaptic vesicle (SV) protein and a candidate gene for autism, the physiological function of SCAMP5 remains mostly enigmatic. Here, using optical imaging and electrophysiological experiments, we demonstrate that SCAMP5 plays a critical role in release site clearance at the active zone. Truncation analysis revealed that the 2/3 loop domain of SCAMP5 directly interacts with adaptor protein 2, and this interaction is critical for its role in release site clearance. Knockdown (KD) of SCAMP5 exhibited pronounced synaptic depression accompanied by a slower recovery of the SV pool. Moreover, it induced a strong frequency-dependent short-term depression of synaptic release, even under the condition of sufficient release-ready SVs. Super-resolution microscopy further proved the defects in SV protein clearance induced by KD. Thus, reduced expression of SCAMP5 may impair the efficiency of SV clearance at the active zone, and this might relate to the synaptic dysfunction observed in autism.**

## INTRODUCTION

Secretory carrier membrane proteins (SCAMPs) are tetraspanin membrane proteins found in secretory and endocytic compartments, and they are implicated in a variety of membrane trafficking events. SCAMPs span the synaptic vesicle (SV) membrane four times with their amino- and carboxy-terminal tails exposed on the cytoplasmic surface of the SV membrane, and they belong to a family of proteins that includes synaptophysin, synaptogyrin, and synaptoporin (Fernández-Chacón et al., 1999). Of the five currently known SCAMPs, SCAMP1 and 5 are highly expressed in the brain and enriched in SVs (Fernández-Chacón and Südhof, 2000). The lack of an obvious synaptic phenotype in SCAMP1 knockout mice (Fernández-Chacón et al., 1999) raised the possibility of a specialized role for SCAMP5 in synaptic function, although evidence for this has largely been lacking. Recent genetic analysis found that SCAMP5 is silenced on a derivative chromosome and reduced in expression to ~40% in a patient with idiopathic, sporadic autism (Castermans et al., 2010). We also found that knockdown (KD) of endogenous SCAMP5 led to an impairment of SV endocytosis and lowered the threshold of activity at which SV endocytosis becomes unable to compensate for the ongoing exocytosis (Zhao et al., 2014). These results suggest that SCAMP5 might play an important role in regulating synaptic transmission and its dysfunction might be related to the autism phenotype.

Sustained synaptic release is limited by the availability of fusion-competent SVs, and, thus, to maintain the fidelity of neurotransmission, SVs should recycle fast enough to prevent SV pool depletion. Although SV depletion is known as a main cause of synaptic depression, several studies have suggested that clearance of specific release sites in the presynaptic active zone provides spatial availability for release-ready SVs and that this is a major rate-limiting step for sustained synaptic transmission (Neher, 2010; Haucke et al., 2011). Consistent with this notion, recent studies have reported that interfering with the function of endocytic proteins, such as dynamin, intersectin1, synaptophysin, and the μ2 subunit of adaptor protein 2 (AP2), causes a rapid short-term depression (STD) of synaptic transmission, which cannot be explained by vesicle depletion but may be a result of defects in the clearance of SV components from release sites (Rajappa et al., 2016; Hua et al., 2013; Neher, 2010; Hosoi et al., 2009; Sakaba et al., 2013).

Here we found that SCAMP5 directly binds to AP2 via its 2/3 loop domain. SCAMP5 KD in cultured hippocampal neurons results in pronounced synaptic depression and a slower recovery of the recycling SV pool. We also observed a clear stimulation frequency-dependent STD with SCAMP5 KD under conditions of normal availability of release-ready SVs. Super-resolution microscopy further proved the defects in the clearance of newly

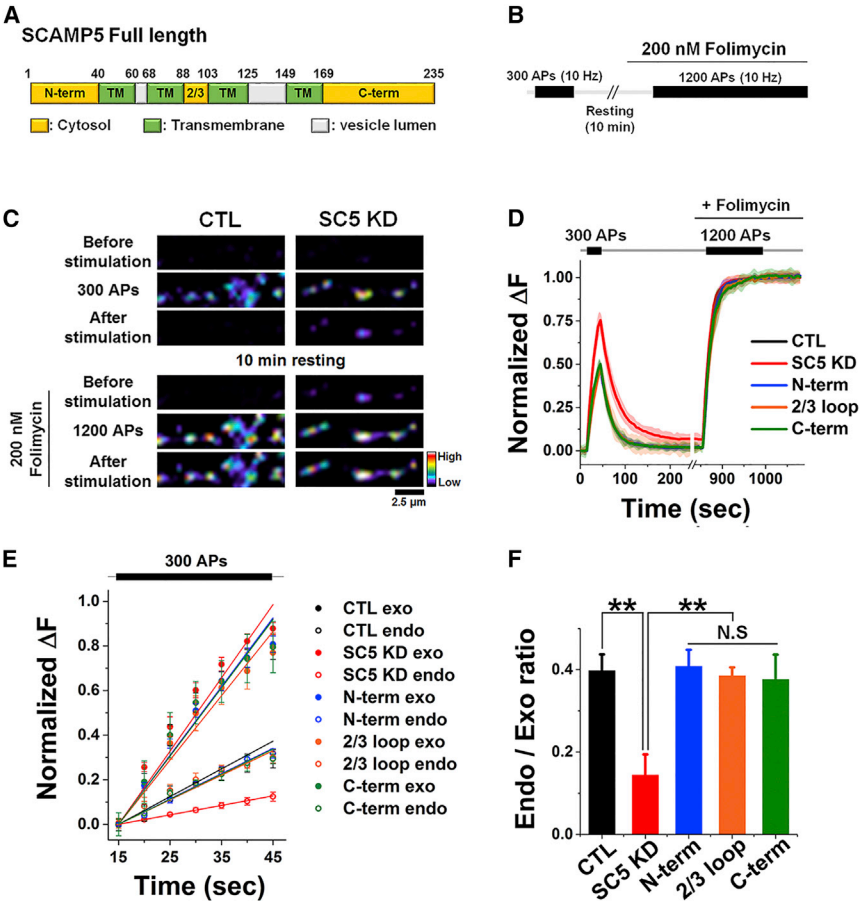


**Figure 1. The Cytoplasmic Domains of SCAMP5 Fail to Phenocopy the Endocytic Defects Caused by SCAMP5 KD**

(A) Schematic image for the SCAMP5 domain structure. Yellow, green, and gray represent cytoplasmic, transmembrane, and vesicle lumen compartments, respectively.

(B) Experimental protocol for pHluorin (vGpH) assay using (C)–(F). Briefly, cultured hippocampal neurons at days in vitro (DIV)16 were stimulated with 300 APs at 10 Hz. After a 10-min resting period, the same neurons were stimulated at 10 Hz for 120 s (1,200 APs) with 200 nM folimycin.

(C) Representative time-lapse vGpH images from control and SCAMP5 KD neurons.

(D) Normalized average vGpH fluorescence intensity profiles from control, SCAMP5 KD, N-terminal domain-overexpressed, 2/3 loop-overexpressed, or C-terminal domain-overexpressed neurons stimulated with or without 200 nM folimycin. The traces in the absence of folimycin represent the balance between exocytosis and endocytosis during stimulation, while those in the presence of folimycin reflect pure exocytosis.

(E) Time course of endocytosis (endo) and exocytosis (exo) during 300-AP (10-Hz) stimulation.

(F) The rates of exocytosis and endocytosis during stimulation were obtained from the linear fits to the initial 30 s of traces (0.40 ± 0.04 for control, 0.14 ± 0.05 for SCAMP5 KD, 0.41 ± 0.04 for N-terminal overexpression, 0.39 ± 0.02 for 2/3 loop overexpression, and 0.38 ± 0.06 for C-terminal overexpression; n > 4 independent experiments).

Values are means ± SEM. N.S., not significant; **p < 0.01 (ANOVA and Tukey's HSD post hoc test). See also Figure S1.

exocytosed synaptotagmin from the active zone by SCAMP5 KD. Our findings indicate that SCAMP5 facilitates release site clearance by interacting with AP2 during high neuronal activity. Reduced expression of SCAMP5 could lead to a traffic jam of vesicular components at release sites and, thereby, contribute to pronounced STD of synaptic transmission during sustained activity.

## RESULTS

### The Cytoplasmic Domains of SCAMP5 Fail to Phenocopy the Endocytic Defects Caused by SCAMP5 KD

We previously showed that SCAMP5 KD results in severe defects in endocytosis during high-frequency stimulation (Zhao et al., 2014). Since SCAMP5 contains three cytoplasmic domains (N-terminal, C-terminal, and 2/3 loop domains; Figure 1A) that could mediate interactions with other proteins, we predicted that overexpression of one of them would phenocopy the effect of SCAMP5 KD as a dominant negative. Neurons were co-transfected with vesicular glutamate transporter-1 fused with pHluorin (vGpH) and SCAMP5-targeted small hairpin RNA (shRNA) or scrambled shRNA. vGpH is a vesicular glutamate transporter-1 fused with pHluorin, a modified GFP with high pH sensitivity (Sankaranarayanan et al., 2000; Voglmaier et al., 2006; Balaji and Ryan, 2007; Burrone et al., 2006), such that its fluorescence is quenched in acidic conditions and increased in basic conditions upon exocytosis to the extracellular space.

Changes in fluorescence levels in the absence of folimycin represent the balance between exocytosis and endocytosis during stimulation, while changes in the presence of folimycin reflect pure exocytosis, enabling the time course of endocytosis during stimulation to be estimated by simply subtracting the fluorescence values (Figures 1B–1E). As previously reported (Zhao et al., 2014), the kinetics of exocytosis were not affected by SCAMP5 KD; therefore, the higher trace in fluorescence in KD indicates severe endocytic defects during stimulation (Figures 1D, 1E, S1A, and S1B). Consistently, the ratio of endocytosis/exocytosis during stimulation, calculated by obtaining the slopes of linear fitted time courses of endocytosis and exocytosis following the 300-action potential (AP) train (Figure 1E), was significantly reduced in SCAMP5 KD neurons compared to control neurons (Figure 1F). None of the three overexpressed cytoplasmic constructs, however, affected the kinetics of endocytosis during stimulation (Figures 1D–1F and S1C).

### SCAMP5 Interacts with AP2-μ2, but YXXϕ Motifs of SCAMP5 Do Not Mediate the Binding

If none of three cytoplasmic domains can phenocopy the endocytic defects observed in SCAMP5 KD, by what mechanism(s) does SCAMP5 KD induce endocytic defects during

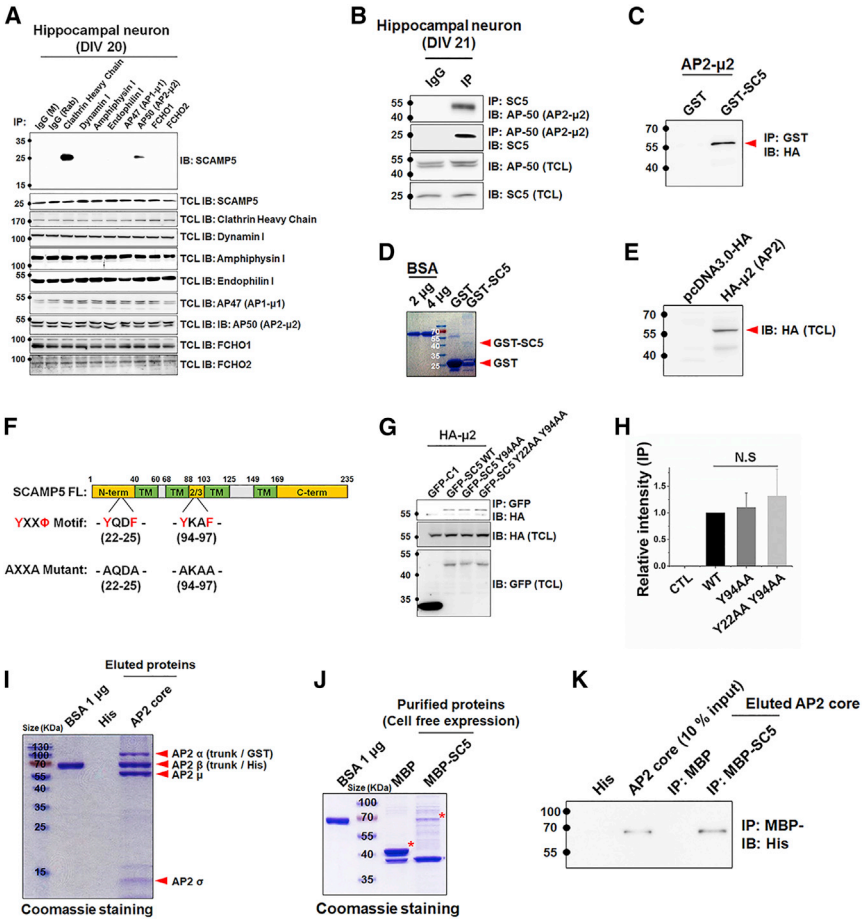


**Figure 2. SCAMP5 Interacts with the AP2 Complex**

(A) Cultured hippocampal neurons at DIV16 were lysed, immunoprecipitated (IP) with various anti-endocytic protein-targeted antibodies, and immunoblotted (IB) with SCAMP5-specific antibody (M, mouse; Rab, rabbit; and TCL, total cell lysates).

(B) Neurons at DIV21 were lysed, immunoprecipitated with anti-SCAMP5 antibody (first panel) or anti-AP-50 (AP2-μ2) antibody (second panel), and immunoblotted with anti-AP-50 antibody (first panel) or anti-SCAMP5 antibody (second panel), respectively.

(C) HEK293T cells were transfected with the HA-μ2 subunit of AP2, lysed, pulled down with purified GST (CTL) or GST- SCAMP5 *in vitro*, and immunoblotted with anti-HA antibody.

(D and E) Amount of purified GST-SCAMP5 and the expression of HA-μ2 were confirmed by Coomassie staining (D) and western blot (E), respectively.

(F) Schematic image indicating the corresponding sequences and locations of YXXϕ motifs at N-terminal and 2/3 loop regions of SCAMP5. Tyrosine and phenylalanine residues at each YXXϕ motif were substituted to alanines to make AXXA mutants.

(G and H) HEK293T cells were cotransfected with the HA-μ2 subunit of AP2 and GFP, GFP-SCAMP5, or GFP-SCAMP5 AXXA mutants (Y94AA and Y22AA/Y94AA); immunoprecipitated with anti-GFP antibody; and immunoblotted with anti-HA antibody. Representative western blot image (G) and quantified data from three independent blots (H). No significant changes were found in the μ2-binding affinity between wild-type (WT) SCAMP5 and AXXA mutant (0 ± 0 for GFP-C1, 1 ± 0 for SCAMP5 WT, 1.10 ± 0.27 for SCAMP5 Y94AA, and 1.31 ± 0.50 for SCAMP5 Y22AA/Y94AA double mutant; n = 3 independent blots).

(I) BL21 cells were co-transformed with GST-α/σ and His-β/μ to purify the AP2 core complex, and the eluted proteins were confirmed by Coomassie gel staining.

(J) Using a cell-free protein expression system, MBP-SCAMP5 was synthesized and purified *in vitro*.

(K) Eluted AP2 core complex was pulled down with purified MBP or MBP-SCAMP5 and immunoblotted with His antibody to identify the direct binding.

Values are means ± SEM. N.S., not significant (ANOVA and Tukey's HSD post hoc test). See also Figure S2.

high-frequency stimulation? To address this question, we conducted immunoprecipitation assays using full-length SCAMP5 to screen potential binding partners. We found that clathrin heavy chain (CHC) and the μ2 subunit of adaptor protein 2 (AP2-μ2) interact with SCAMP5 in cultured hippocampal neurons (Figure 2A).

The interaction between SCAMP5 and AP2 was further confirmed by immunoprecipitation assays using SCAMP5 and AP2-μ2 antibodies and using purified GST-SCAMP5 pull-down (Figures 2B–2E). Tyrosine-based binding motifs (YXXϕ) are important for AP2 binding (Collins et al., 2002; Reider and Wendland, 2011), and SCAMP5 has two YXXϕ motifs at its N-terminal and 2/3 loop domains (Figure 2F). Unexpectedly, however, neither a YXXϕ motif mutant (AXXA) at the N-terminal nor that at the 2/3 loop domain prevented SCAMP5 from binding to AP2-μ2 (Figures 2G and 2H).

AP2 is a heterotetrameric adaptor composed of α, β, μ, and σ subunits, and the N-terminal domains of all 4 AP2 subunits form a tightly interlinked core structure comprised of a dimer of dimers between the α/σ and β/μ subunits (Collins et al., 2002). To investigate whether the AP2 core complex directly binds to SCAMP5, the AP2 core complex was assembled by coexpression of two bicistronic vectors (trunk domains of α [1–621] and σ/trunk domains of β [1–591] and μ) in BL21 (Collins et al., 2002) and purified (Figure 2I). We also have purified MBP-SCAMP5 using a cell-free protein expression system (Figure 2J). We found that SCAMP5 binds directly to the AP2 core complex (Figure 2K), but not to the other well-known AP2-binding protein sorting nexin 9 (SNX9) (Figures S2A–S2C) or the N-terminal domain of CHC (Figures S2D–S2H).

We further identified the AP2-μ2-interacting region of SCAMP5 (Figures 3A–3C). Unlike the full length of SCAMP5, none of the 3 cytoplasmic domains, including the N-terminal, C-terminal, and 2/3 loop, binds to AP2-μ2, which explains the observation that none of them affected endocytic kinetics when overexpressed (Figures 1 and 3B). Intriguingly, our results revealed that only the 2/3 loop domain, flanked by a transmembrane domain on each of its N- and C-terminal sides (TM-2/3-TM), binds to AP2-μ2 (Figure 3C). The 2/3 loop domain containing only one transmembrane domain on either the N- or

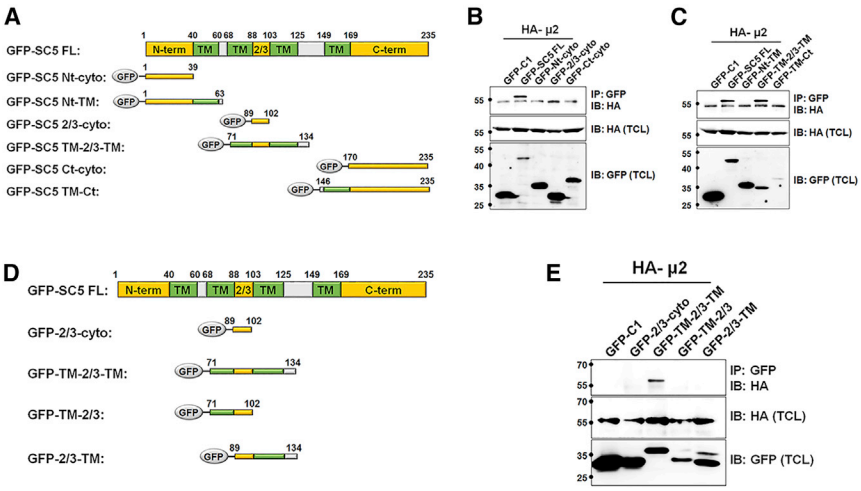


**Figure 3. The 2/3 Loop Domain Flanked by a Transmembrane Domain on Each of Its N- and C-terminal Sides Is Critical for the Binding of SCAMP5 to AP2**

(A) Domain organization of SCAMP5 and various GFP-tagged truncation mutant constructs used in (B) and (C).

(B and C) HEK293T cells were transfected with HA-μ2 and GFP or GFP-tagged proteins, immunoprecipitated with anti-GFP antibody, and immunoblotted with anti-HA antibody.

(B) None of the cytosolic truncation mutants binds AP2-μ2.

(C) The 2/3 loop domain flanked by a transmembrane domain on each of its N- and C-terminal sides (TM-2/3-TM) only binds to AP2-μ2.

(D) Schematic image of transmembrane deletion mutants used in (E).

(E) The 2/3 loop domain flanked by a transmembrane domain on each of its N- and C-terminal sides (TM-2/3-TM) only binds to AP2-μ2, while the 2/3 loop domain containing one on either N- or C-terminal side or none of the transmembrane domains (2/3-cyto, TM-2/3, or 2/3-TM) fails to bind.

C-terminal side (TM-2/3 or 2/3-TM) failed to do so (Figures 3D and 3E). Collectively, these results indicated that a distinct structural element of the 2/3 loop domain flanked by a transmembrane domain on each of its N-terminal and C-terminal sides is required for the binding of SCAMP5 to AP2.

## SCAMP5 KD in Neurons Causes Fast Synaptic Depression

We investigated the physiological significance of SCAMP5 by performing whole-cell voltage-clamp recordings in autaptic cultures of dissociated hippocampal neurons (Figure 4A). We locally stimulated neurons by delivering electrical pulses to the cell body using a stimulating electrode, and we recorded evoked excitatory postsynaptic currents (EPSCs) from the same cell body of the autaptic neurons (Zhou et al., 2000; Liu et al., 2009).

Since we previously showed that SCAMP5 KD lowered the threshold of activity at which SV endocytosis becomes unable to compensate for the ongoing exocytosis during high-frequency stimulation (Zhao et al., 2014), we first tested whether SCAMP5 plays a role in maintaining the recycling SV pool during sustained neuronal activity. When a train of AP-like stimuli was applied to the presynaptic terminal, the EPSC showed a depression but reached a steady state within 10 stimuli, reflecting a balance between SV usage and recruitment of new SVs. At 5-Hz frequency of stimulation, although EPSC amplitude after 10 stimuli was reduced to ~60% of the initial stimulus, no difference in the steady-state EPSCs between control and SCAMP5 KD was found (Figures 4B and 4C). At 10-Hz stimulation, however, a difference between control and SCAMP5 KD neurons emerged and became more pronounced at later time points; by the end of a train, practically no EPSCs were elicited in KD neurons, leading to pronounced synaptic depression during sustained high neuronal activity (Figures 4D and 4E).

We further measured the time course of recovery of the recycling SV pool. Neurons were stimulated at 20 Hz for 2 s to deplete vesicles, and, after a brief pause, they were stimulated at 3 Hz for 2 s and 2 and 1 Hz for 1 s each to monitor the recovery of EPSCs (Figure 4F). Amplitudes of all responses were normalized to the final response after 3 s of the recovery period (Figure 4F). During 2-s stimulation at 3 Hz, the capacities of recovery from SV depletion in both control and KD neurons were rapidly saturated but at a significantly lower level in KD neurons, as compared to control neurons (Figures 4F and 4G).

## KD of Endogenous SCAMP5 Induces Frequency-Dependent STD

Recent studies suggest that blocking endocytosis causes a rapid form of stimulation frequency-dependent STD as the result of slow clearance of SV components from the release sites within the active zone (Rajappa et al., 2016; Hua et al., 2013; Neher, 2010). The severe impairment of endocytosis during high-frequency stimulation and the pronounced synaptic depression in SCAMP5 KD neurons prompted us to test the possibility that the endocytic defects in SCAMP5 KD might lead to an inefficient clearance of vesicular components at release sites and, thereby, contribute to synaptic depression during sustained activity.

We conducted experiments with a pre-pulse normalization protocol to prevent a bias caused by different initial release probability and inhomogeneous probe expression level (Rajappa et al., 2016; Hua et al., 2013). Neurons co-expressing SCAMP5 shRNA/scrambled shRNA and vGpH were stimulated with 50-AP (20-Hz) test pulse, and then 200 APs at 5, 10, 20, or 40 Hz were given after 50-s intervals in the presence of folimycin to measure the amount of exocytosis (Figure 5A).

In control neurons, the similarity among cumulative amplitudes of the total fluorescence increases each at 5, 10, and 20 Hz (with a slight decrease at 40 Hz) was observed. In SCAMP5 KD, however, the amplitude of fluorescence responses dropped with increasing stimulation frequency, indicating strong STD at 10, 20, and 40 Hz, but not at 5 Hz (Figures 5B–5F), which is consistent with our findings of a more pronounced depression in KD (Figure 4). Significant STD was again observed with an

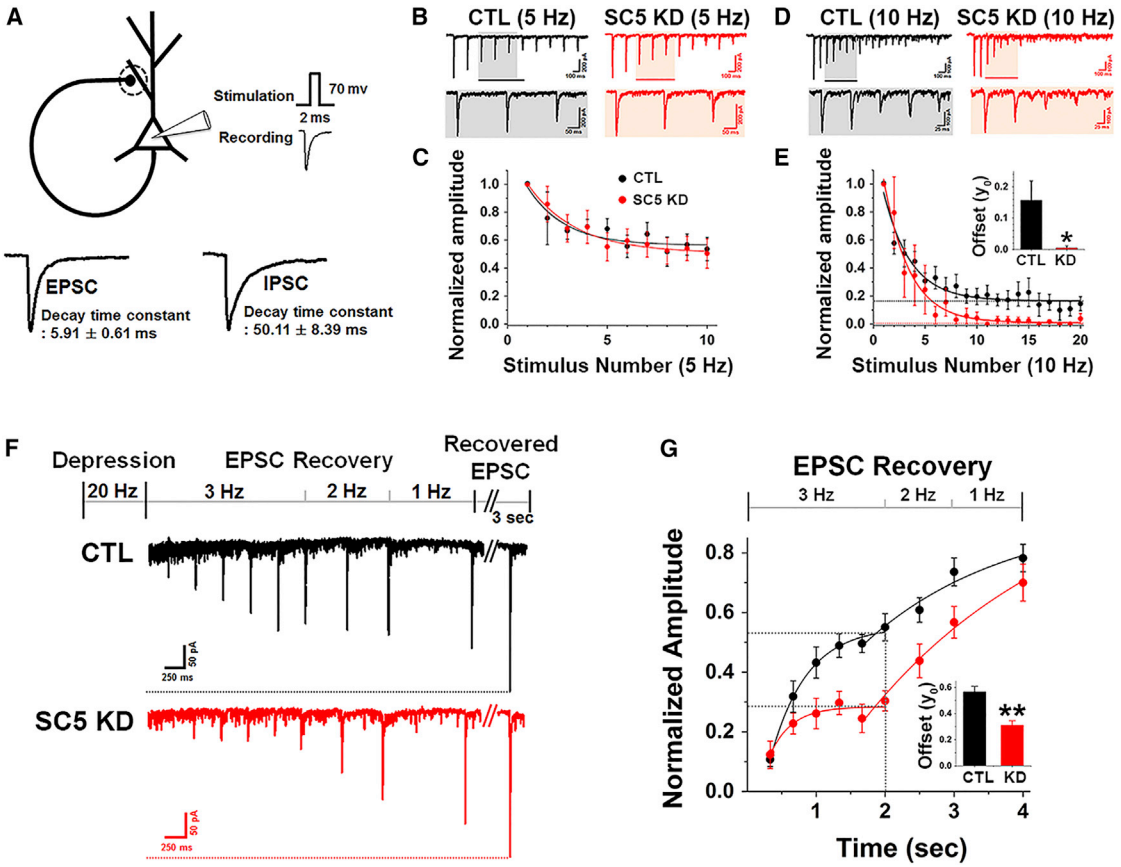


**Figure 4. SCAMP5 KD in Hippocampal Autaptic Neurons Showed Fast Synaptic Depression and Slow EPSC Recovery**

(A) Schematic figure of hippocampal autaptic neurons for whole-cell voltage-patch clamp. AP-like stimulus (+70 mV for 2 ms) was applied, and postsynaptic currents were measured simultaneously with same patch pipette. Although both evoked excitatory and inhibitory postsynaptic currents (EPSCs and IPSCs) were obtained, only EPSCs, which have a faster decay time constant than that of IPSCs, were recorded and analyzed.

(B–G) Autaptic neurons were infected with AAV-U6-GFP-scrambled shRNA or AAV-U6-GFP-SCAMP5-targeted shRNA at DIV4. All experiments were performed at DIV16.

(B) Representative traces of evoked EPSCs in control (scrambled shRNA) and SCAMP5 KD during 2-s stimulation at 5 Hz. Shaded areas were magnified for clarity.

(C) Normalized EPSC amplitude plot in control (black, n = 5 neurons) and SCAMP5 KD (red, n = 7 neurons) neurons. Amplitude values were normalized to the first response in the train.

(D) Representative traces of EPSCs in control (scrambled shRNA) and SCAMP5 KD during 2-s stimulation at 10 Hz. Pronounced synaptic depression emerged in both control and SCAMP5 KD neurons but did so much faster in KD neurons.

(E) Normalized amplitude plots were fitted with single-exponential function (offset values: 0.157 ± 0.061 for control [n = 5 neurons] and 0.009 ± 0.005 for SCAMP5 KD [n = 6 neurons]).

(F and G) EPSCs were fully depressed with a train at 20 Hz for 2 s and gradually recovered.

(F) Representative recordings of EPSC recovery after synaptic depression in control (scrambled shRNA) and SCAMP5 KD. Neurons were stimulated at 3, 2, and 1 Hz. Amplitudes of all responses were normalized to the final response after 3 s of the recovery period.

(G) Normalized EPSC amplitudes at 3 Hz fitted with a single-exponential function revealed the plateaus at which the capacities of recovery were saturated, but at a significantly lower level in SCAMP5 KD neurons than in control neurons (0.567 ± 0.041 for CTL and 0.311 ± 0.034 for SCAMP5 KD).

n = 10 neurons for control, n = 6 neurons for KD. Values are means ± SEM. *p < 0.05 and **p < 0.01 (Student's t test).

alternative SV probe, synaptophysin-pH (Figure S3), and with an independent shRNA (shRNA2) (Figures S4A–S4D). In addition, STD at 10 Hz was fully rescued by coexpression of an shRNA-resistant form of SCAMP5 in KD neurons (Figures S4E–S4H).

The STD described above could be due to either lack of release-ready SVs or defects in SV release site clearance. We first measured the size of readily releasable pool (RRP) and recycling pool. As we previously reported (Zhao et al., 2014), the recycling pool size was slightly reduced, but the size of RRP was not affected by SCAMP5 KD (Figure S5). To test whether SV pool depletion is the cause for STD in KD, we analyzed SV exocytic response after repetitive 50 APs at 20-Hz stimulus at 50-s intervals in the presence of folimycin. Since post-stimulus endocytosis in SCAMP5 KD is largely unaffected (Zhao et al., 2014), we expected that a 50-s interval is enough for post-stimulus endocytosis to occur. During the repeated 50-AP stimulus trains,

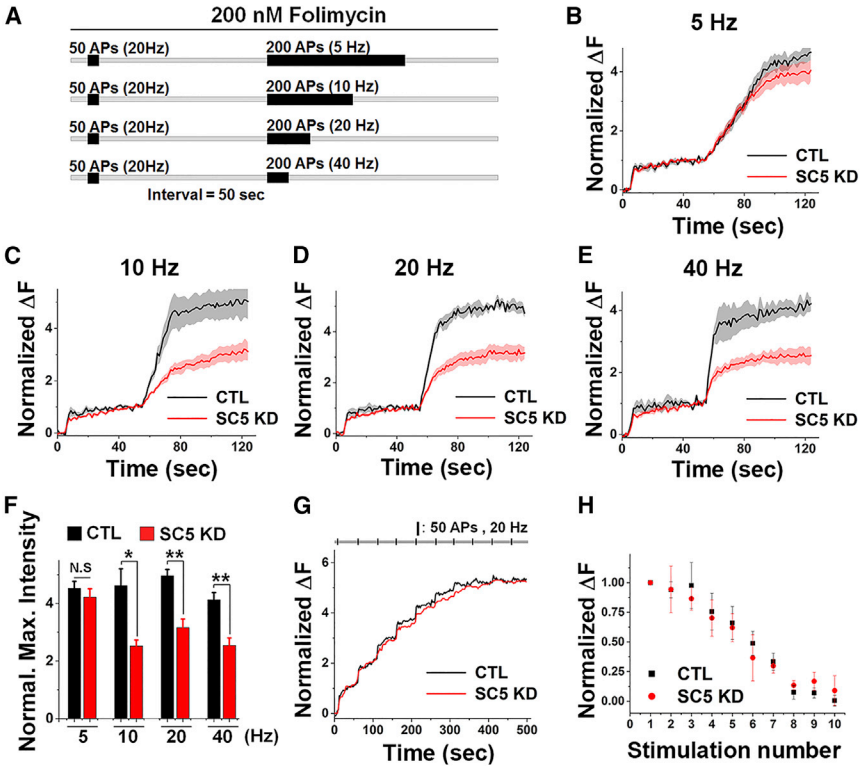


**Figure 5. SCAMP5 KD Induces a Frequency-Dependent Rapid STD**

(A) Experimental protocols. Neurons co-expressing vGpH and scrambled shRNA or SCAMP5-targeted shRNA (pSiren-U6) were treated with 200 nM folimycin and stimulated with 50 action potentials (APs) at 20 Hz as a calibration stimulus. After a 50-s interval, the second stimulus (200 APs) was given with the different frequencies (5, 10, 20, and 40 Hz).

(B–E) Averaged vGpH response in control (black) and SCAMP5 KD (red) neurons to 50 APs at 20 Hz followed by 200 APs at 5 Hz (B), 10 Hz (C), 20 Hz (D), and 40 Hz (E). Fluorescence response was normalized to the value obtained from the calibration stimulus (50 APs at 20 Hz). Note the strong STD in SCAMP5 KD after stimulation with 10, 20, and 40 Hz, but not with 5 Hz.

(F) Normalized maximum intensity (Normal. Max. Intensity) was calculated by averaging the last 10 points of vGpH responses. Fluorescence response was normalized to the value obtained from the calibration stimulus (4.52 ± 0.24 for CTL 5 Hz [n = 4 independent experiments], 4.22 ± 0.29 for SCAMP5 KD 5 Hz [n = 5 independent experiments]; 4.62 ± 0.59 for CTL 10 Hz [n = 5 independent experiments], 2.52 ± 0.21 for SCAMP5 KD 10 Hz [n = 4 independent experiments]; 4.97 ± 0.21 for CTL 20 Hz [n = 5 independent experiments], 3.16 ± 0.30 for SCAMP5 KD 20 Hz [n = 6 independent experiments]; 4.12 ± 0.25 for CTL 40 Hz [n = 4 independent experiments], 2.54 ± 0.26 for SCAMP5 KD 40 Hz [n = 4 independent experiments]).

(G) Exemplary vGpH responses of control (black) and SCAMP5 KD (red) to consecutive stimuli of 50 APs at 20 Hz with 50-s intervals in the presence of 200 nM folimycin (n = 6 independent experiments for CTL and SCAMP5 KD). Traces are normalized to the first response. Black bars indicate the stimulation time.

(H) Plot of normalized fluorescence increment upon each trial from the experiments shown in (G). In control and SCAMP5 KD neurons, the responses were decreased to 0.0054 ± 0.045 and 0.0898 ± 0.1259, respectively.

Values are means ± SEM. N.S., not significant; *p < 0.05 and **p < 0.01 (Student's t test). See also Figures S3–S5.

RRPs for each subsequent release are composed of a portion of recycled SVs (alkaline-trapped SVs) and SVs from the reserve pool. Thus, fluorescence responses are decreased gradually due to an increasing percentage of alkaline-trapped SVs in the RRP, which cannot contribute to a fluorescence increase during subsequent stimulation (Rajappa et al., 2016). A progressive reduction of fluorescence responses is comparable in control neurons and in SCAMP5 KD neurons, indicating that SVs are replenished similarly via either recruitment from the reserve pool or recycling of previously released SVs in both groups (Figures 5G and 5H). These results suggest that STD in SCAMP5 KD is a result of defects in release site clearance rather than a lack of available SVs (Figures 5G and 5H).

## Interaction between the 2/3 Loop Domain of SCAMP5 and AP2 Is Critical for Its Function in the Release Site Clearance

To directly assess whether AP2 binding is critical for the SCAMP5 function in the release site clearance, we constructed an AP2-binding-defective mutant SCAMP5. Any mutants encompassing the 2/3 loop domain with N-terminal- and C-terminal-sided transmembrane domains, however, failed to be expressed. We circumvented this issue by designing full-length SCAMP5 containing randomly scrambled 14 amino acids in the 2/3 loop of SCAMP5 (SC5 $FL^{scr\ 2/3\ loop}$; Figure 6A). We confirmed that this mutation did not change the overall tetra-membrane-spanning topology of wild-type SCAMP5 (SC5 $FL^{WT}$) (Figure 6B) and did not bind to AP2-μ2 (Figure 6C) but still was able to bind synaptotagmin (Han et al., 2009) (Figure S6). We then constructed an shRNA-resistant form of the scrambled mutant (SC5 $FL^{scr\ 2/3\ loop}$ resi; Figure 6D), and we performed rescue experiments. The shRNA-resistant scrambled mutant was expressed in the presynaptic boutons similar to the shRNA-resistant form of wild-type SCAMP5 (Figure 6E); but, unlike wild-type, it failed to rescue the defects in release site clearance caused by SCAMP5 KD (Figures 6F and 6G). These results suggest that AP2 binding to the 14 amino acids of the SCAMP5 2/3 loop is critical for the role of SCAMP5 in the release site clearance.

## Super-Resolution Microscopy Visually Reveals the Defects in Release Site Clearance by SCAMP5 KD

To prove the direct relationship between SCAMP5 and release site clearance, we took advantage of super-resolution microscopy, using stochastic optical reconstruction microscopy (STORM) along with an appropriate staining protocol. Neurons co-expressing synaptotagmin-pHluorin (Stg-pH) and SCAMP5-targeted shRNA or scrambled shRNA were treated with

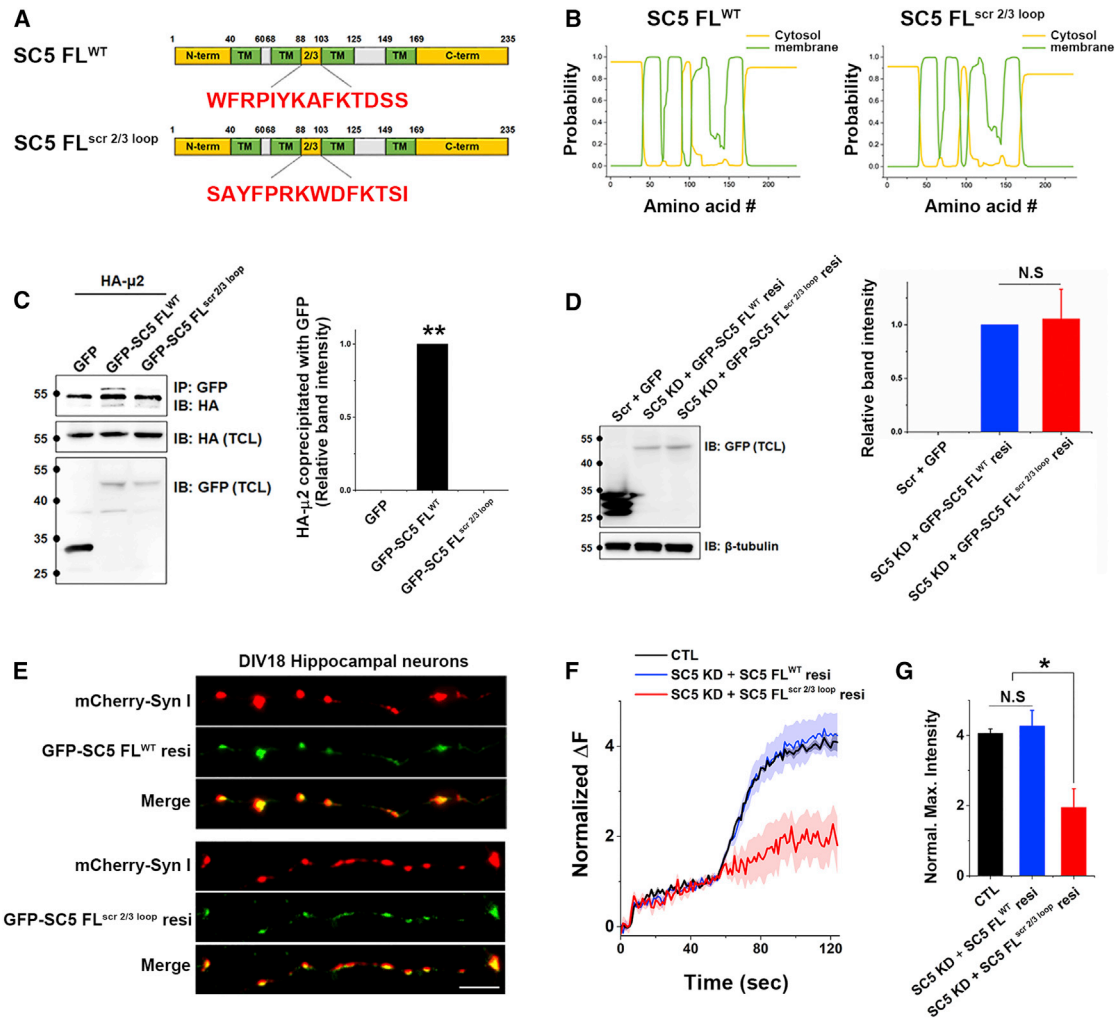


**Figure 6. SCAMP5 and AP2 Binding Is Critical for Release Site Clearance**

(A) Schematic image indicating the corresponding sequences of wild-type SCAMP5 (SC5 $FL^{WT}$) and scrambled cytosolic 2/3 loop mutants SCAMP5 ($SC5^{scr\ 2/3\ loop}$).

(B) Prediction of transmembrane helices in proteins using a TMHMM v.2.0.

(C) HEK293T cells were co-transfected with HA-μ2 and GFP-SC5 $FL^{WT}$ or GFP-$SC5^{scr\ 2/3\ loop}$ for 48 hr and lysed for immunoprecipitation. Lysates were pulled down with GFP antibody and immunoblotted with HA antibody (0 ± 0 for GFP, 1 ± 0 for GFP-SC5 $FL^{WT}$, and 0 ± 0 for GFP-$SC5^{scr\ 2/3\ loop}$ [n = 3 independent blots]).

(D) The shRNA-resistant form of GFP-SC5 $FL^{WT}$ (GFP-SC5 $FL^{WT}$ resi) or GFP-$SC5^{scr\ 2/3\ loop}$ (GFP-$SC5^{scr\ 2/3\ loop}$ resi) was transfected with SCAMP5-targeted shRNA in HEK293T cells for 72 hr and lysed for western blot. The intensity of band was normalized to that of GFP-SC5 $FL^{WT}$ resi (0 ± 0 for Scr + GFP, 1 ± 0 for SC5 KD + GFP-SC5 $FL^{WT}$ resi, and 1.05 ± 0.28 for SC5 KD + GFP-$SC5^{scr\ 2/3\ loop}$ resi [n = 4 independent blots]).

(E) Presynaptic expression of GFP-SC5 $FL^{WT}$ resi and GFP-$SC5^{scr\ 2/3\ loop}$ resi. Neurons were co-transfected with mCherry-synapsin I (mCherry-Syn I) and GFP-SC5 $FL^{WT}$ resi or GFP-$SC5^{scr\ 2/3\ loop}$ resi at DIV8 and imaged at DIV16. Scale bar, 5 μm.

(F) Averaged vGpH response in control (vGpH + pSiren-U6-scrambled shRNA + SBFP2-C1; black), SCAMP5 KD + SC5 $FL^{WT}$ resi (vGpH + pSiren-U6-shRNA + SBFP2-SC5 $FL^{WT}$ resi; blue), and SCAMP5 KD + $SC5^{scr\ 2/3\ loop}$ resi (vGpH + pSiren-U6-shRNA + SBFP2-$SC5^{scr\ 2/3\ loop}$ resi; red) neurons to 50 APs at 20 Hz followed by 200 APs at 10 Hz. Fluorescence response was normalized to the value obtained from the calibration stimulus (50 APs at 20 Hz).

(G) Normalized maximum intensity was calculated by averaging the last 10 points of vGpH responses (4.06 ± 0.13 for control [n = 3 independent experiments], 4.26 ± 0.45 for SCAMP5 KD + SC5 $FL^{WT}$ resi [n = 5 independent experiments], and 1.95 ± 0.53 for SCAMP5 KD + $SC5^{scr\ 2/3\ loop}$ resi [n = 4 independent experiments]).

Values are means ± SEM. N.S., not significant; *p < 0.05 and **p < 0.01 (Student's t test for C and D and ANOVA and Tukey's HSD post hoc test for G). See also Figure S6.

unlabeled GFP nanobody to mask the surface Stg-pH fraction. Neurons were then stimulated with 200 APs at 20 Hz in the presence of Alexa-647-conjugated GFP nanobody to label newly exocytosed Stg-pH, and they were further incubated for 50 s after stimulation to allow time for release site clearance, followed by immediate fixation on ice. Fixed neurons were then stained with a specific antibody against the active zone marker, bassoon followed by Alexa-568 secondary antibody (Figure 7A).

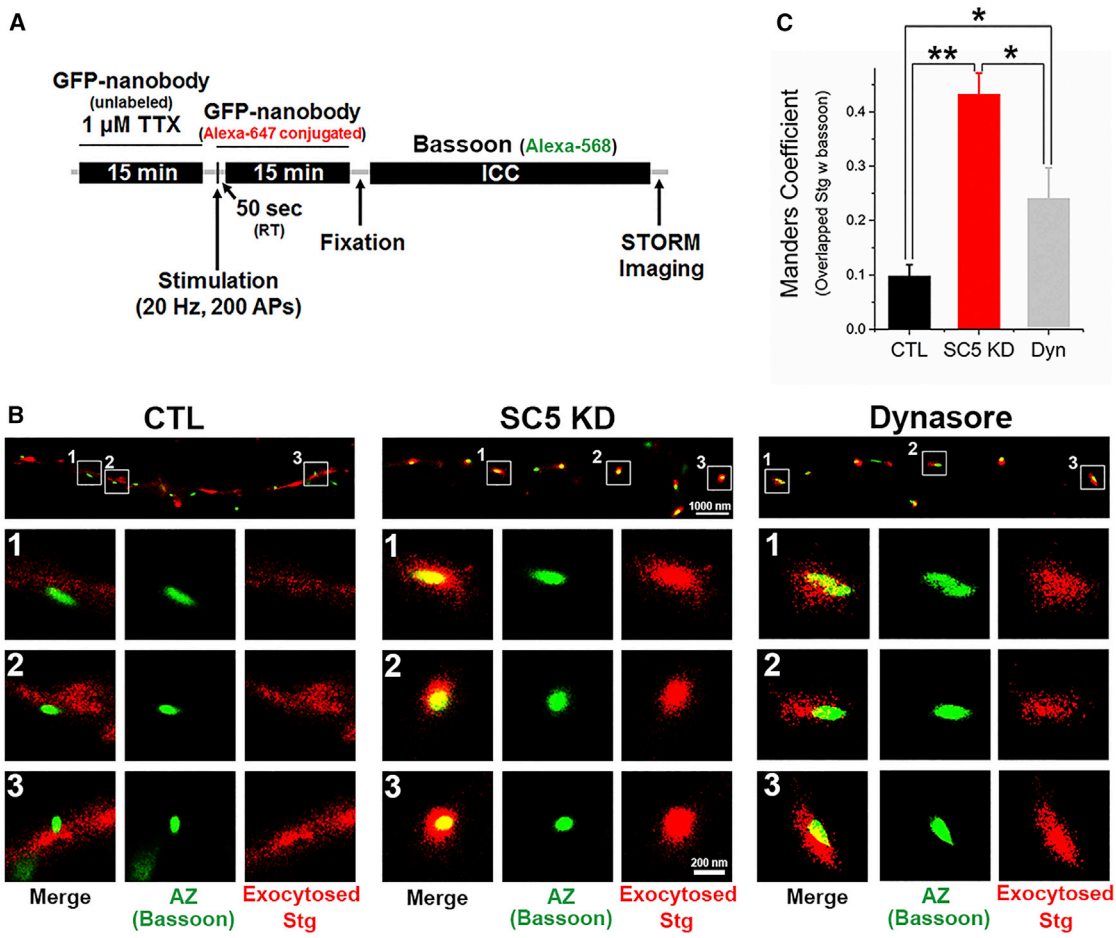


**Figure 7. Super-resolution Microscopy Reveals the Defects in the Release Site Clearance by SCAMP5 KD**

(A) Experimental protocols for dual-color STORM imaging.

(B) Representative STORM images of control, SCAMP5 KD, and dynasore- (100 μM) treated neurons. Green, bassoon (stained with Alexa-568-conjugated antibody); red, exocytosed synaptotagmin-pHluorin (Stg, labeled with Alexa-647-conjugated GFP nanobody). Scale bar, 1 μm (200 nm for enlarged images).

(C) Manders coefficients were calculated from each STORM image (proportion of overlap of 647 channel [exocytosed Stg-pH] with 568 channel [bassoon]: 0.098 ± 0.021 for CTL [n = 6 independent experiments], 0.432 ± 0.039 for SCAMP5 KD [n = 5 independent experiments], and 0.241 ± 0.056 for CTL with dynasore [Dyn, n = 5 independent experiments]).

Values are means ± SEM. *p < 0.05 and **p < 0.01 (ANOVA and Tukey's HSD post hoc test). See also Figure S7.

Dual-color STORM imaging showed that the immunoreactivity of newly exocytosed Stg-pH was well dispersed bi-laterally and clearly separated from that of bassoon in control neurons, indicating the movement of exocytosed Stg-pH to the periactive zone (Figure 7B). In marked contrast, Stg-pH signals in SCAMP5 KD were found mostly within the active zone, thus being highly colocalized with bassoon, indicating that they completely failed to move laterally to the periactive zone (Figures 7B and 7C). Consistently, we found that strong STD was observed with Stg-pH in SCAMP5 KD and that SCAMP5 KD did not lead to an increase in the surface level of stranded Stg in the resting state (Figures S7A–S7D). We further demonstrated that endogenously expressed synaptotagmin behaved similarly to overexpressed Stg-pH using STORM imaging (Figures S7E–S7H).

To gain further insight into the role of SCAMP5 in release site clearance, we treated neurons with dynasore to inhibit dynamin, a key protein in SV endocytosis and vesicle (or endosome) scission, and we performed STORM imaging to compare it to the result with SCAMP5 KD (Figures 7B and 7C). As previously reported (Hua et al., 2013), Stg-pH signals in dynasore-treated neurons were found to be in proximity with bassoon signals (Figure 7B). The degree of colocalization between Stg-pH and bassoon, however, was significantly lower than that in SCAMP5 KD (Figure 7C). This result suggests that SCAMP5 KD strongly perturbs translocation of Stg-pH toward the periactive zone by inhibiting the early phase of endocytosis that happens before SV scission mediated by dynamin.

Taken together, our imaging data strongly support our electrophysiology and pHluorin assays, and they suggest that SCAMP5 has an important role in maintaining synaptic transmission by facilitating SV release site clearance. Binding to AP2 through its 2/3 loop could underpin a molecular mechanism for the role

of SCAMP5 in release site clearance during high-frequency stimulation.

## DISCUSSION

SCAMP5 is highly expressed in neurons, and reduced expression of SCAMP5 may be related to synaptic dysfunction observed in patients with autism (Castermans et al., 2010; Fernández-Chacón and Südhof, 2000); but, its exact cellular and molecular functions are mostly unknown. We found that SCAMP5 directly interacts with the AP2 core complex via its 2/3 loop domain flanked by a transmembrane domain on each of its N- and C-terminal sides. Reduction of SCAMP5 expression causes pronounced synaptic depression and a slower recovery of the recycling SV pool. Using pHluorin-based live-cell imaging and super-resolution microscopy, we observed a clear stimulation frequency-dependent STD in SCAMP5 KD neurons due to defects in clearance of release sites within the active zone. These results suggest that the endocytic defects in SCAMP5 KD might lead to a traffic jam of vesicular components at release sites and, thereby, contribute to synaptic depression during sustained activity.

Since SCAMP5 KD induced defects in SV endocytosis at high-frequency stimulation, we tested whether SCAMP5 is associated with endocytic proteins, and we found interactions with the AP2 complex and CHC as a result. The AP2 complex is a well-known adaptor protein that links cargo proteins to clathrin-coated pits and has four different subunits ($\alpha$, $\beta$, $\mu$, and $\sigma$ subunits) (Reider and Wendland, 2011). AP2 can bind to various endocytic cargoes and clathrin via distinct binding motifs. For example, the $\alpha$ subunit binds to various endocytic accessory proteins that have Dx[F/W], FxDxF, or WVxF motifs (Owen et al., 1999; Traub et al., 1999). The $\beta$2 subunit of the AP2 complex binds to clathrin via its LLNLD in the hinge domain and to a dileucine motif [D/E]xxL[LI] in the cargo molecules. Furthermore, the $\mu$2 subunit binds to YXX$\phi$ motifs and WVxF found in stonin2 (Doray et al., 2007; Kelly et al., 2008; Owen et al., 2004). Although SCAMP5 interacts with the AP2 complex, none of the cytoplasmically located parts of SCAMP5 (N-terminal, C-terminal, and 2/3 loop regions) mediates this interaction. This could explain the lack of any of their inhibitory effects on SV endocytosis. Furthermore, although the N-terminal (22–25 amino acids [aa]) and 2/3 loop domain (94–97 aa) of SCAMP5 have consensus AP2-$\mu$2-binding YXX$\phi$ motifs, single- and double-point mutants (Y22AA/Y94AA) of SCAMP5 were still able to bind AP2-$\mu$2. We even tested whether FRPI (FXX$\phi$, the structurally similar motif for YXX$\phi$) residue at 90–93 aa can mediate the interaction between SCAMP5 and AP2-$\mu$2, since other SCAMP isoforms (SCAMP1, 2, and 3) contain a canonical YRPI/M (YXX$\phi$) residue at the corresponding regions (data not shown). We found that none of them affected the interaction between SCAMP5 and AP2-$\mu$2. Eventually, using a cell-free protein expression system for *in vitro* transcription and translation of SCAMP5, we demonstrated that the AP2 core complex binds directly to SCAMP5.

Interestingly, the 2/3 loop domain flanked by a transmembrane domain on each of its N- and C-terminal sides (TM-2/3-TM) was the only truncation that was able to bind AP2, while the 2/3 loop domain containing either one or none of transmembrane domains failed to do so. Although this domain does not conform to any of the known AP2-binding consensus sequences, we believe that this is not a very rare occurrence. Indeed, a recent study has shown that intersectin1 SH3A-B linker domain directly interacts with AP2-$\alpha$ and -$\beta$ subunits via noncanonical hydrophobic peptides (Pechstein et al., 2010). We designed a full-length mutant SCAMP5 containing 14 amino acids randomly scrambled in the 2/3 loop domain of SCAMP5, and we proved that this mutant is defective in AP2 binding and fails to rescue the phenotype caused by SCAMP5 KD. Interestingly, a recent study has revealed that AP2-$\mu$2 functionally binds to the C2 domain of otoferlin, a cargo protein of an inner hair cell (IHC), and facilitates the clearance of release sites (Jung et al., 2015). Impairment of AP2 function increases the number of endosome-like vacuoles and decreases the number of clathrin-coated membrane and distal SVs (Jung et al., 2015). In addition, the fast onset of exocytosis defects in AP2-$\mu$2-disrupting cells supports the idea that AP2-$\mu$2 performs not only in SV regeneration but also active zone replenishment (Jung et al., 2015). Given the selective interaction between full-length SCAMP5 and AP2 and the functional role of the AP2-$\mu$2 subunit for release site clearance, we conclude that the interaction between SCAMP5 and AP2 plays a key role in release site clearance and SV endocytosis during high-frequency stimulation.

Release site clearance is the process that rapidly clears the exocytosed material from the release site to enable new rounds of vesicle docking and release (Neher, 2010). It is known as the rate-limiting step for release of SVs, and a delay in such clearance processes may result in STD of synaptic transmission (Neher, 2010). The rate of release site clearance is determined by the speed of which SV components are swept away from the fusion site toward the periactive zone, where endocytic retrieval occurs. Since exocytosis and endocytosis are tightly coupled, impairing endocytosis leads to a rapid STD as a result of slow clearance of release sites.

A recent study showed that clathrin and AP2 are not essential for SV retrieval at the plasma membrane but mediate SV reformation from internal endosomes (Kononenko et al., 2014). We, however, believe that this remains a subject of much debate. Using repetitive 50 APs at 20-Hz stimulus at 50-s intervals, we found that STD in SCAMP5 KD is not due to insufficient available SV supply (Figures 5G and 5H). In addition, STORM imaging also showed that SCAMP5 KD perturbs translocation of Stg-pH toward the periactive zone by inhibiting an earlier phase of endocytosis than the SV scission step (Figure 7). Therefore, even though there might be some defects in SV reformation at the levels of endosomes, the resulting shortage of SV would have contributed negligibly to the strong STD observed in SCAMP5 KD.

As we previously found in SCAMP5 KD neurons, the endocytic capacity to cope with heavy exocytic loads is reduced, whereas the endocytosis activity of individual SVs during mild exocytic loads remains largely unaffected (Zhao et al., 2014). Previous studies in dynamin-1 and synaptophysin knockout mice also found a selective requirement for dynamin-1 and synaptophysin when an intense stimulus imposed a heavy load on endocytosis (Ferguson et al., 2007; Kwon and Chapman, 2011). Another study showed that loss of synaptophysin 1 induces frequency-dependent STD, and, therefore, synaptophysin 1 is essential for synaptobrevin 2 clearance to prevent STD (Rajappa et al.,

2016). Although it is not clear whether SCAMP5 also has a direct role in the lateral diffusion of exocytosed materials, our results from pHluorin and super-resolution imaging suggest that, together with synaptophysin, SCAMP5 interacts with AP2 (and possibly with dynamin-1) to form the key endocytic machinery that is critical for maintaining an adequate endocytosis, particularly during intense stimulation.

SCAMP5, together with neurobeachin (NBEA) and syntaxin-binding protein 6 (AMISYN), has been identified as a candidate gene for autism that is involved in the secretion of large dense-core vesicles (Castermans et al., 2010), thus suggesting that the regulation of neuronal vesicle trafficking may be involved in the pathogenesis of autism, although underlying molecular mechanisms remain unknown. With the results from the current study and a previous one (Zhao et al., 2014), we suggest that SCAMP5 is a critical regulator of SV endocytosis and release site clearance, particularly during intense neuronal activity. Reduction in SCAMP5 expression may lead to a defect in the clearance process of exocytosed SV components, leading to rapid short-term release depression. Therefore, our results uncover a molecular mechanism underlying pre-synaptic dysfunction associated with SCAMP5 reduction, which might provide a molecular target for synaptic dysfunction observed in autism.

## EXPERIMENTAL PROCEDURES

For further details, see the Supplemental Experimental Procedures.

### Plasmid DNA Construction

The vGpH, Stg-pH, AP2 core complex, pET21a-CHC, and His-Stg plasmids were kindly provided by colleagues (see the Supplemental Experimental Procedures). SCAMP5-targeted shRNAs from the rat SCAMP5 sequence (NM_031726) were cloned into the pSiren-U6-mRFP vector or adeno-associated virus (AAV)-U6-GFP (or SBFP2) vector. The targeting sequence is 54–74 bp for shRNA1 and 657–677 bp for shRNA2. The shRNA-resistant form of SCAMP5 was constructed by point mutation. pET MBP His6 LIC cloning vector (2Cc-T) was from Addgene (plasmid 37237), and 6xHis-tag was deleted using PCR for the AP2 core complex-binding assay. For AAV production, annealed oligonucleotide of shRNA or scrambled RNA was cloned into the AAV vector, and AAV was produced as previously described (Guo et al., 2012; Lee et al., 2016).

### Antibodies

A list of antibodies used in this study is provided in the Supplemental Experimental Procedures.

### Cell Culture and Transfection

Hippocampal neurons were prepared from embryonic day 18 rat embryos, cultured, and transfected as previously described (Park et al., 2017). All of the animal experiments were performed according to the IACUC (Institute of Animal Care and Use Committee) guidelines of Seoul National University (SNU-111104-5). HEK293T cells were transfected by GeneIn transfection reagent following the manufacturer's instructions. Autaptic neurons were prepared as previously described (Bekkers and Stevens, 1991; Burgalossi et al., 2012) with several modifications. In brief, stamps for micro-islands were generated by spraying a mixture of poly-D-lysine and rat tail collagen on glass coverslips. Glial cells were plated on coverslips and grown on micro-islands, and then dissociated hippocampal neurons were plated on top at low density ($2.5 \times 10^4$ cells).

### Electrophysiology

Whole-cell patch-clamp recordings were carried out using autaptic hippocampal neurons grown on micro-islands. GFP-positive neurons were voltage-clamped at −70 mV, and AP-like stimuli (+70 mV for 2 ms) were applied using an EPC-8 amplifier, filtered at 3 kHz and sampled at 10 kHz, and PULSE software (HEKA Electronic). Patch pipettes were filled with pipette internal solution (130 mM potassium gluconate, 20 mM KCl, 10 mM K-HEPES, 0.2 mM EGTA, 0.3 mM Na-GTP, and 4 mM Mg-ATP [pH 7.3]; 285–290 mOsm). The extracellular solution comprised 148 mM NaCl, 10 mM glucose, 2 mM $CaCl_2$, 1 mM $MgCl_2$, 2.5 mM KCl, 10 mM HEPES (pH 7.4) (285–290 mOsm). The data were analyzed using IGOR Pro (Wavemetrics) and Origin 9 software (OriginLab).

### Image Acquisition

Coverslips were mounted in a perfusion/stimulation chamber equipped with platinum-iridium field stimulus electrodes, and neurons were stimulated (1 ms, 20–50 V, bipolar) using a current stimulator. Time-lapse images were acquired with a Nikon Eclipse Ti-U microscopy with a 40×, 1.0 numerical aperture (NA) oil lens using an Andor iXon 897 electron multiplying charge-coupled device (EMCCD) camera. The neurons were continuously perfused at room temperature with tyrode solution containing the following (in mM): 136 NaCl, 2.5 KCl, 2 $CaCl_2$, 1.3 $MgCl_2$, 10 HEPES, and 10 glucose (pH 7.3), and 10 μM 6-cyano-7-nitroquinoxaline-2,3-dione (CNQX) and 50 μM DL-2-amino-5-phosphonopentanoic acid (APV) were added to prevent recurrent excitation during stimulation. The exocytosis/endocytosis assay using pHluorin was performed as described previously (Park et al., 2017; Zhao et al., 2014).

### Protein Purification, Western Blot, and Immunoprecipitation

Each construct was transformed into BL21 cells and grown at 37°C. Cells were induced protein expression and lysed with hypotonic buffer (20 mM Tris-HCl [pH 8], 150 mM NaCl, 1 mM EGTA, 1 mM $MgCl_2$, 1% Triton X-100, and 0.1% sodium deoxycholate [DOC]) for GST proteins or Ni-NTA lysis buffer (50 mM $NaH_2PO_4$, 300 mM NaCl, and 10 mM Imidazole) for 6xHis proteins. After centrifugation, the supernatant was incubated with GST (GE Healthcare Life Science) or Ni-NTA (Incospharm) beads. For the *in vitro* binding assay, 6xHis proteins were eluted using elution buffer (50 mM $NaH_2PO_4$, 300 mM NaCl, and 300 mM Imidazole). pET-MBP-SCAMP5 or pET-6xHis-MBP-SCAMP5 was synthesized with AccuRapid Cell-Free protein expression kit following the manufacturer's instruction (Bioneer). We followed the previously described western blot and immunoprecipitation protocols (Park et al., 2017).

### Topology Prediction

Structural predictions were performed using Transmembrane Hidden Markov Model (TMHMM version [v.]2.0) (Krogh et al., 2001).

### Dual-Color STORM Imaging

STORM images of the neurons were captured by an N-STORM (Nikon, Tokyo, Japan) microscope using 100× total internal reflection fluorescence (TIRF) objective lens (1.4 NA) and an iXon3 897 EMCCD (Andor Technologies) in the STORM imaging buffer (690 μL 50 mM Tris-HCl [pH 8], 10 mM NaCl, and 10% glucose with 7 μL 0.56 mg/mL glucose oxidase, 3.4 mg/mL catalase in 10 mM Tris-HCl [pH 8], 50 mM NaCl, and 7 μL beta-mercaptoethanol). The STORM imaging cycle (1 activation/4 acquisition) was repeated 1,500 times for each channel. The data were analyzed using Thunder-STORM plugin (Ovesný et al., 2014), and colocalization of dual-color STORM images was analyzed with Manders coefficient after background subtraction using ImageJ.

### Statistical Analysis

Statistical analysis was performed with SPSS v.19 (IBM). Kolmogorov-Smirnov normality test was used to check the normality of data. If normality assumption was confirmed, Student's two-sample t test was used to compare two independent groups. For multiple conditions, we compared mean values by ANOVA followed by Tukey's honest significant difference (HSD) post hoc test or Fisher's least significant difference (LSD) test (depending on the number of groups).

## SUPPLEMENTAL INFORMATION

Supplemental Information includes Supplemental Experimental Procedures and seven figures and can be found with this article online at https://doi.org/10.1016/j.celrep.2018.02.088.

## ACKNOWLEDGMENTS

This research was supported by grants from Korea-UK R&D Collaboration Project (HI14C2229) to S.C. by the Ministry of Health and Welfare, South Korea.

## AUTHOR CONTRIBUTIONS

D.P. and S.C. designed the experiments. D.P., U.L., E.C., H.Z., J.A.K., and B.J.L. performed the experiments. D.P., U.L., W.-K.H., K.C., and S.C. analyzed the data. D.P., U.L., J.A.K., P.R., K.C., and S.C. wrote the paper.

## DECLARATION OF INTERESTS

The authors declare no competing interests.

Received: August 17, 2017
Revised: January 19, 2018
Accepted: February 22, 2018
Published: March 20, 2018

## REFERENCES

Balaji, J., and Ryan, T.A. (2007). Single-vesicle imaging reveals that synaptic vesicle exocytosis and endocytosis are coupled by a single stochastic mode. Proc. Natl. Acad. Sci. USA *104*, 20576–20581.

Bekkers, J.M., and Stevens, C.F. (1991). Excitatory and inhibitory autaptic currents in isolated hippocampal neurons maintained in cell culture. Proc. Natl. Acad. Sci. USA *88*, 7834–7838.

Burgalossi, A., Jung, S., Man, K.N., Nair, R., Jockusch, W.J., Wojcik, S.M., Brose, N., and Rhee, J.S. (2012). Analysis of neurotransmitter release mechanisms by photolysis of caged $Ca^{2+}$ in an autaptic neuron culture system. Nat. Protoc. *7*, 1351–1365.

Burrone, J., Li, Z., and Murthy, V.N. (2006). Studying vesicle cycling in presynaptic terminals using the genetically encoded probe synaptopHluorin. Nat. Protoc. *1*, 2970–2978.

Castermans, D., Volders, K., Crepel, A., Backx, L., De Vos, R., Freson, K., Meulemans, S., Vermeesch, J.R., Schrander-Stumpel, C.T., De Rijk, P., et al. (2010). SCAMP5, NBEA and AMISYN: three candidate genes for autism involved in secretion of large dense-core vesicles. Hum. Mol. Genet. *19*, 1368–1378.

Collins, B.M., McCoy, A.J., Kent, H.M., Evans, P.R., and Owen, D.J. (2002). Molecular architecture and functional model of the endocytic AP2 complex. Cell *109*, 523–535.

Doray, B., Lee, I., Knisely, J., Bu, G., and Kornfeld, S. (2007). The gamma/sigma1 and alpha/sigma2 hemicomplexes of clathrin adaptors AP-1 and AP-2 harbor the dileucine recognition site. Mol. Biol. Cell *18*, 1887–1896.

Ferguson, S.M., Brasnjo, G., Hayashi, M., Wölfel, M., Collesi, C., Giovedi, S., Raimondi, A., Gong, L.W., Ariel, P., Paradise, S., et al. (2007). A selective activity-dependent requirement for dynamin 1 in synaptic vesicle endocytosis. Science *316*, 570–574.

Fernández-Chacón, R., and Südhof, T.C. (2000). Novel SCAMPs lacking NPF repeats: ubiquitous and synaptic vesicle-specific forms implicate SCAMPs in multiple membrane-trafficking functions. J. Neurosci. *20*, 7941–7950.

Fernández-Chacón, R., Alvarez de Toledo, G., Hammer, R.E., and Südhof, T.C. (1999). Analysis of SCAMP1 function in secretory vesicle exocytosis by means of gene targeting in mice. J. Biol. Chem. *274*, 32551–32554.

Guo, P., El-Gohary, Y., Prasadan, K., Shiota, C., Xiao, X., Wiersch, J., Paredes, J., Tulachan, S., and Gittes, G.K. (2012). Rapid and simplified purification of recombinant adeno-associated virus. J. Virol. Methods *183*, 139–146.

Han, C., Chen, T., Yang, M., Li, N., Liu, H., and Cao, X. (2009). Human SCAMP5, a novel secretory carrier membrane protein, facilitates calcium-triggered cytokine secretion by interaction with SNARE machinery. J. Immunol. *182*, 2986–2996.

Haucke, V., Neher, E., and Sigrist, S.J. (2011). Protein scaffolds in the coupling of synaptic exocytosis and endocytosis. Nat. Rev. Neurosci. *12*, 127–138.

Hosoi, N., Holt, M., and Sakaba, T. (2009). Calcium dependence of exo- and endocytotic coupling at a glutamatergic synapse. Neuron *63*, 216–229.

Hua, Y., Woehler, A., Kahms, M., Haucke, V., Neher, E., and Klingauf, J. (2013). Blocking endocytosis enhances short-term synaptic depression under conditions of normal availability of vesicles. Neuron *80*, 343–349.

Jung, S., Maritzen, T., Wichmann, C., Jing, Z., Neef, A., Revelo, N.H., Al-Moyed, H., Meese, S., Wojcik, S.M., Panou, I., et al. (2015). Disruption of adaptor protein 2μ (AP-2μ) in cochlear hair cells impairs vesicle reloading of synaptic release sites and hearing. EMBO J. *34*, 2686–2702.

Kelly, B.T., McCoy, A.J., Späte, K., Miller, S.E., Evans, P.R., Höning, S., and Owen, D.J. (2008). A structural explanation for the binding of endocytic dileucine motifs by the AP2 complex. Nature *456*, 976–979.

Kononenko, N.L., Puchkov, D., Classen, G.A., Walter, A.M., Pechstein, A., Sawade, L., Kaempf, N., Trimbuch, T., Lorenz, D., Rosenmund, C., et al. (2014). Clathrin/AP-2 mediate synaptic vesicle reformation from endosome-like vacuoles but are not essential for membrane retrieval at central synapses. Neuron *82*, 981–988.

Krogh, A., Larsson, B., von Heijne, G., and Sonnhammer, E.L. (2001). Predicting transmembrane protein topology with a hidden Markov model: application to complete genomes. J. Mol. Biol. *305*, 567–580.

Kwon, S.E., and Chapman, E.R. (2011). Synaptophysin regulates the kinetics of synaptic vesicle endocytosis in central neurons. Neuron *70*, 847–854.

Lee, S.E., Kim, Y., Han, J.K., Park, H., Lee, U., Na, M., Jeong, S., Chung, C., Cestra, G., and Chang, S. (2016). nArgBP2 regulates excitatory synapse formation by controlling dendritic spine morphology. Proc. Natl. Acad. Sci. USA *113*, 6749–6754.

Liu, H., Dean, C., Arthur, C.P., Dong, M., and Chapman, E.R. (2009). Autapses and networks of hippocampal neurons exhibit distinct synaptic transmission phenotypes in the absence of synaptotagmin I. J. Neurosci. *29*, 7395–7403.

Neher, E. (2010). What is Rate-Limiting during Sustained Synaptic Activity: Vesicle Supply or the Availability of Release Sites. Front. Synaptic Neurosci. *2*, 144.

Ovesný, M., Křížek, P., Borkovec, J., Svindrych, Z., and Hagen, G.M. (2014). ThunderSTORM: a comprehensive ImageJ plug-in for PALM and STORM data analysis and super-resolution imaging. Bioinformatics *30*, 2389–2390.

Owen, D.J., Vallis, Y., Noble, M.E., Hunter, J.B., Dafforn, T.R., Evans, P.R., and McMahon, H.T. (1999). A structural explanation for the binding of multiple ligands by the alpha-adaptin appendage domain. Cell *97*, 805–815.

Owen, D.J., Collins, B.M., and Evans, P.R. (2004). Adaptors for clathrin coats: structure and function. Annu. Rev. Cell Dev. Biol. *20*, 153–191.

Park, D., Na, M., Kim, J.A., Lee, U., Cho, E., Jang, M., and Chang, S. (2017). Activation of CaMKIV by soluble amyloid-$\beta_{1-42}$impedes trafficking of axonal vesicles and impairs activity-dependent synaptogenesis. Sci. Signal. *10*, eaam8661.

Pechstein, A., Bacetic, J., Vahedi-Faridi, A., Gromova, K., Sundborger, A., Tomlin, N., Krainer, G., Vorontsova, O., Schäfer, J.G., Owe, S.G., et al. (2010). Regulation of synaptic vesicle recycling by complex formation between intersectin 1 and the clathrin adaptor complex AP2. Proc. Natl. Acad. Sci. USA *107*, 4206–4211.

Rajappa, R., Gauthier-Kemper, A., Böning, D., Hüve, J., and Klingauf, J. (2016). Synaptophysin 1 Clears Synaptobrevin 2 from the Presynaptic Active Zone to Prevent Short-Term Depression. Cell Rep. *14*, 1369–1381.

Reider, A., and Wendland, B. (2011). Endocytic adaptors–social networking at the plasma membrane. J. Cell Sci. *124*, 1613–1622.

Sakaba, T., Kononenko, N.L., Bacetic, J., Pechstein, A., Schmoranzer, J., Yao, L., Barth, H., Shupliakov, O., Kobler, O., Aktories, K., and Haucke, V. (2013). Fast neurotransmitter release regulated by the endocytic scaffold intersectin. Proc. Natl. Acad. Sci. USA *110*, 8266–8271.

Sankaranarayanan, S., De Angelis, D., Rothman, J.E., and Ryan, T.A. (2000). The use of pHluorins for optical measurements of presynaptic activity. Biophys. J. *79*, 2199–2208.

Traub, L.M., Downs, M.A., Westrich, J.L., and Fremont, D.H. (1999). Crystal structure of the alpha appendage of AP-2 reveals a recruitment platform for clathrin-coat assembly. Proc. Natl. Acad. Sci. USA *96*, 8907–8912.

Voglmaier, S.M., Kam, K., Yang, H., Fortin, D.L., Hua, Z., Nicoll, R.A., and Edwards, R.H. (2006). Distinct endocytic pathways control the rate and extent of synaptic vesicle protein recycling. Neuron *51*, 71–84.

Zhao, H., Kim, Y., Park, J., Park, D., Lee, S.E., Chang, I., and Chang, S. (2014). SCAMP5 plays a critical role in synaptic vesicle endocytosis during high neuronal activity. J. Neurosci. *34*, 10085–10095.

Zhou, Q., Petersen, C.C., and Nicoll, R.A. (2000). Effects of reduced vesicular filling on synaptic transmission in rat hippocampal neurones. J. Physiol. *525*, 195–206.